POLITECNICO DI TORINO
Repository ISTITUZIONALE

Magnetic history effects on DC shielding performance of Bi-2223 and Bi-2223/Fe coaxial cups

Original
Magnetic history effects on DC shielding performance of Bi-2223 and Bi-2223/Fe coaxial cups / Fracasso, M., Gerbaldo, R., Ghigo, G., Fagnard, J., Vanderbemden, P., Gozzelino, L.. - In: SUPERCONDUCTOR SCIENCE & TECHNOLOGY. - ISSN 1361-6668. - 39:10(2026), pp. 1-17. [10.1088/1361-6668/aeaddb]

Availability:
This version is available at: 11583/3016881 since: 2026-10-22T13:43:31Z

Publisher:
IOP

Published
DOI:10.1088/1361-6668/aeaddb

Terms of use:

This article is made available under terms and conditions as specified in the corresponding bibliographic description in the repository

Publisher copyright

(Article begins on next page)

12 November 2026

Superconductor
Science and
Technology

PURPOSE-LED
PUBLISHING™

PAPER • **OPEN ACCESS**

Magnetic history effects on DC shielding performance of Bi-2223 and Bi-2223/Fe coaxial cups

To cite this article: M Fracasso *et al* 2026 *Supercond. Sci. Technol.* **39** 105016

View the article online for updates and enhancements.

You may also like

- Critical current densities and the effects of thermally assisted flux flow in single crystals of $Bi_2Sr_2CaCu_2O_8$
J van den Berg, C J van der Beek, P H Kes et al.

- Shielding efficiency and *E*(*J*) characteristics measured on large melt cast Bi-2212 hollow cylinders in axial magnetic fields
J-F Fagnard, S Elschner, J Bock et al.

- Screening of magnetic fields by superconducting and hybrid shields with a circular cross-section
Laura Gozzelino, Michela Fracasso, Mykola Solovyov et al.

kiutra

Millikelvin characterization for superconducting devices

L-TYPE RAPID

- **< 4 hrs** sample loading and cooldown to base
- **50 mK** base temperature
- **30 min** warm up and sample exchange

Find out more →



This content was downloaded from IP address 192.135.30.4 on 22/10/2026 at 14:39

Superconductor Science and Technology

Check for updates

OPEN ACCESS

RECEIVED
30 May 2026

REVISED
16 September 2026

ACCEPTED FOR PUBLICATION
29 September 2026

PUBLISHED
13 October 2026

Original content from this work may be used under the terms of the Creative Commons Attribution 4.0 licence.

Any further distribution of this work must maintain attribution to the author(s) and the title of the work, journal citation and DOI.

PAPER

Magnetic history effects on DC shielding performance of Bi-2223 and Bi-2223/Fe coaxial cups

M Fracasso[1,2,*], **R Gerbaldo**[1,2], **G Ghigo**[1,2], **J-F Fagnard**[3], **P Vanderbemden**[3] and **L Gozzelino**[1,2]

[1] Department of Applied Science and Technology, Politecnico di Torino, Torino, Italy
[2] Istituto Nazionale di Fisica Nucleare, Sezione di Torino, Torino, Italy
[3] Department of Electrical Engineering and Computer Science, Montefiore Institute B28, University of Liège, B-4000 Liège, Belgium
[*] Author to whom any correspondence should be addressed.

E-mail: michela.fracasso@polito.it

Keywords: magnetic shielding, magnetic history effects, hybrid superconducting/ferromagnetic shields, Bi-2223

Abstract

The DC magnetic shielding properties of a commercial Pb-doped $Bi_2Sr_2Ca_2Cu_3O_{10+x}$ (Bi-2223) cup were investigated under axial, transverse, and crossed magnetic field configurations. Particular attention was devoted to the role of the magnetization history, which was shown to significantly influence the ability to shield a magnetic field applied orthogonal to the direction of the first magnetization process. A progressive reduction of the shielding capability was observed with increasing field applied in the pre-magnetization process, revealing distinct regimes associated with the evolution of the internal current distribution. The superimposition of a ferromagnetic (FM) cup was found not only to strongly increase the maximum shielded field—from 8.2 to 144 mT in the transverse orientation and from 11.5 to 68 mT in the axial orientation—but also to markedly reduce these history dependent effects, leading to a more stable shielding performance over a wide range of pre-magnetization field values. To understand these results, a three-dimensional numerical approach based on the vector potential (**A**) formulation was developed and validated by comparing the computational output with the experimental data. The simulations provide insight into the underlying mechanisms, highlighting the competition between magnetization-induced and shielding currents and their impact on the final current density distribution. These findings clarify the role of magnetization history in Bi-2223 magnetic shielding and demonstrate the effectiveness of hybrid superconducting/FM configurations for improving performance under realistic operating conditions.

1. Introduction

Magnetic shielding is of primary importance in several technological applications requiring a controlled magnetic environment. These include superconducting (SC) devices, particle accelerators, high-sensitivity measurement systems such as SQUID-based detectors, as well as applications in quantum computing, biomedical engineering, and space missions [1–10]. In this context, superconductors provide an efficient solution as passive shields, exploiting their intrinsic ability to generate persistent currents that produce magnetic fields opposing to the applied field. Consequently, regions with a significant reduction in the magnetic flux density can be established [11]. The maximum field that can be shielded depends strongly on the operating temperature, the SC material and its geometry. For example, for bulk hollow cylinders with bore sizes larger than 1 cm, shielded fields up to 2 T at 4.2 K for MgB_2, 1.4 T at 4.2 K for Bi-2212, and 1.8 T at 77 K for YBCO have been reported [12–14]. However, these high shielded fields are generally obtained at temperatures well below 77 K and over relatively small shielded volumes. Moreover, at high operating fields, SC shields can be affected by thermomagnetic instabilities. Flux jumps, which can abruptly degrade their shielding performance, have, for example, been reported in MgB_2 shields [15, 16] and Nb_3Sn shields [17–19]. High-temperature superconducting (HTS) materials are particularly attractive because of their ability to provide strong attenuation of magnetic fields, especially in the

© 2026 The Author(s). Published by IOP Publishing Ltd

low-frequency and quasi-static regimes, where conventional ferromagnetic (FM) shields may become less effective under high-field conditions. Moreover, cuprate HTS materials can operate at liquid nitrogen temperature, thus enabling the use of simpler and more cost-effective cryogenic systems [20–23].

Among HTS materials, Bi-based compounds, and in particular $Bi_2Sr_2Ca_2Cu_3O_{10+x}$ (Bi-2223), represent a promising solution for shielding applications. Although at 77 K Bi-2223 shields generally exhibit shielded fields of less than a few tens of millitesla [24–27], their polycrystalline nature enables the industrial production of large, continuous components with tubular or more complex geometries [28, 29]. These characteristics, together with their stable shielding response at liquid nitrogen temperature, make Bi-2223 suitable for magnetic shielding applications with practical relevance. Moreover, several strategies can be adopted to improve the shielding performance of Bi-2223 shields. For instance, the choice of closed-end geometries, such as single-capped cylindrical tubes, can enhance the shielding efficiency to a variable extent depending on the field orientation [30]. Additionally, hybrid SC/FM layouts exploiting the complementary effects of magnetic flux shielding by the superconductor and flux deflection through the ferromagnet can be employed [31–34]. On the other hand, the shielding performance of HTS materials is strongly affected by their magnetic history. When an external magnetic field exceeding the lower critical field is applied, vortices start to penetrate the superconductor and can become pinned within the material, leading to trapped magnetic flux and persistent current distributions [35]. Consequently, the resulting magnetic state depends not only on the instantaneous applied magnetic field, but also on the previous magnetization history [36, 37]. This aspect becomes particularly relevant under realistic operating conditions, where magnetic fields may be applied sequentially along different orientations. In such cases, the shielding properties in one direction can be altered by the presence of magnetizing currents induced in the material by previously applied magnetic fields. Although cross-field (CF) and magnetization history effects in HTS materials have been extensively discussed in the literature [38–40], their specific impact on bulk HTS magnetic shields has received comparatively limited experimental attention. Wéra *et al* [41] investigated the effect of an initial trapped field on the shielding performance of an open Bi-2223 tube. For all the investigated magnetizing configurations, they identified three different regimes as the magnetizing field was increased: an initial plateau in which the shielding performance remained unaffected, a progressive decrease of the shielding performance, and a second plateau associated with the fully magnetized state. Their results therefore demonstrated that the shielding performance against a field applied along one direction can be significantly degraded by a previous magnetization along an orthogonal direction.

Building on the findings of Wéra *et al* [41], in this work the shielding performance of a commercial Pb-doped Bi-2223 tube with a closed end (hereinafter referred to as the SC cup) was investigated both when used alone as a SC shield and when coaxially inserted into an outer single-capped Fe tube (i.e. a FM cup) to form a hybrid SC+FM shield. The main objective was therefore twofold: to investigate the effect of the magnetic history on the shielding properties of a closed-end geometry and to determine whether and how the superimposition of an outer FM cup modifies this effect. The influence of magnetic history was investigated by applying a magnetizing field perpendicular to the subsequently applied shielding field, hereinafter referred to as the CF configuration. Two CF configurations were considered: (i) axial pre-magnetization followed by transverse shielding measurements, and (ii) transverse pre-magnetization followed by axial shielding measurements. In addition, measurements in purely axial (AF) and purely transverse (TF) field configurations were also performed for comparison. Normalized parameters, analogous to those adopted in [41], were used as a convenient means of comparing the pre-magnetization level and the resulting degradation in shielding performance under different field orientations and shield configurations.

In this context, numerical modelling plays a key role in understanding the physical mechanisms governing flux penetration, current redistribution, and magnetization processes, as well as in optimizing the shielding performance of SC devices [42, 43]. Among the available approaches, the finite element method (FEM) is widely used to model SC and FM materials by solving Maxwell's equations at the macroscopic level, typically assuming homogeneous material properties [44–46]. In this framework, the SC behaviour is typically described through its *E-J* (electric field-current density) characteristic [11, 47], while the FM response is introduced via its nonlinear *B-H* (magnetic flux density—magnetic field) characteristic or its magnetic permeability μ_r [46, 48]. To obtain a more complete understanding, the experimental study was therefore supported by a computational investigation. We used a FEM-based software employing a magnetic vector potential (**A**) formulation [49, 50] to model both the Bi-2223 and the FM shield. This numerical approach was validated through a comparison of the numerical results with the experimental data. The model was then exploited to gain insight into the magnetic state of the SC shield, with particular focus on the distribution of the magnetization-process-induced current density and trapped magnetic flux, and their impact on the shielding response, under different pre-magnetization

conditions. This computational analysis was also used to clarify how the outer FM cup modifies the SC current redistribution and mitigates the magnetic history effects observed in the SC cup alone.

This paper is structured as follows: the experimental procedures are described in section 2, while the results are presented in section 3. In particular, the shielding characterization of the zero-field cooled (ZFC) shields in the AF and TF orientations is illustrated in section 3.1, while the effect of a previous magnetization in the CF condition is discussed in section 3.2. In section 4, the modelling approach, its validation, and the computational results are presented. Finally, the main conclusions are summarized in section 5.

2. Experimental procedures

The Bi-2223 cup is a polycrystalline single-capped tube with a hemispherical bottom (fabricated by CAN Superconductors, model CSV-12), with the following dimensions: inner radius $R_{i,SC} = 6.01$ mm, inner height $h_{i,SC} = 43.40$ mm, lateral thickness $t_l = 1.58$ mm, and bottom thickness $t_b = 1.68$ mm (figure 1(a)). According to the manufacturer, Bi-2223 magnetic shields of the CSV series have a nominal critical temperature of 110 K and a nominal shielded magnetic flux density exceeding 5 mT at 77 K [51].

The FM cup is made of ARMCO iron, and its dimensions are: inner radius $R_{i,FM} = 8.76$ mm, inner height $h_{i,FM} = 48.58$ mm, and thickness $t_{FM} = 1.75$ mm (figure 1(b)). It was coaxially superimposed to the SC cup in such a way that the lateral wall of the FM cup protruded beyond the aperture of the SC cup by $\Delta h = 3.50$ mm. The radial gap between the two cups, ΔR, was 1.17 mm, while the axial gap between their bottom surfaces, Δt_b, was zero at the shield's symmetry axis and increased with radial distance because of the hemispherical shape of the SC cup bottom (figure 1(c)). The FM cup relative permeability at low fields exceeds $\mu_r = 7500$, while its saturation magnetic flux density is approximately 2.3 T and it was preliminarily degaussed by means of a thermal treatment in vacuum at 760 °C for 1 h. A degaussing procedure was also performed after each characterization process by applying magnetic fields of alternating polarity and progressively decreasing amplitude. Starting from the magnitude of the maximum field applied in the shielding characterization, the $\mu_0 H_{app}$ amplitude was reduced by 3 mT at each step down to 1 mT and then by 0.1 mT down to zero. At each step, positive and negative fields were applied successively and held for 5 s each.

2.1. Measurement details

The shielding properties of the SC and hybrid (SC+FM) shields were preliminarily investigated under ZFC conditions. The shields were cooled down from ambient temperature (T_{amb}) to 77 K by placing them in a liquid nitrogen bath. The cryostat was then positioned in a homogeneous external magnetic field, which was applied either parallel (AF) or perpendicular (TF) to the sample axis.

For the characterization in CF orientation, the ZFC samples were first magnetized by applying a field $\mu_0 H_{app,magn}$ along the axial (or transverse) direction, after which the field was reduced to zero. Then, keeping the samples at 77 K, their shielding properties were investigated by applying a magnetic field perpendicular to the previous one. In other words, the magnetization cycle was performed after ZFC condition, whereas shielding characterization was carried out in CF condition. For the sake of clarity, the procedure is schematically illustrated in figure 2. Moreover, for simplicity, the notation AF and TF is retained throughout the paper to denote the orientation of the applied magnetic field, including in CF experiments.

The magnetic field was supplied by a Kepco BOP 50-20MG power supply connected to a solenoidal electromagnet for the AF orientation and to a Helmholtz coil for the TF orientation. A constant ramp rate of $dB/dt = 1$ mT s^{-1} was used in both field orientations. The magnetic flux density was measured using a cryogenic Arepoc® Axis-3S Hall probe, which was oriented to detect the component of the magnetic flux density parallel to the applied field, namely B_z in AF orientation and B_y in TF orientation. In both orientations and for both the SC and the hybrid shields, the magnetic flux density was measured along the shield's axis placing the Hall probe at ≈ 10 mm above the bottom of the SC cup (position hp_0). For the SC cup alone, in AF orientation and ZFC condition, B_z was also measured along the cup axis at position hp_1, i.e. in correspondence to the open edge of the shield, 43.40 mm above its bottom. The measurement in the latter position was used to estimate the critical current density, as described in section 4. The Hall probe voltage was acquired using a LabVIEW program.

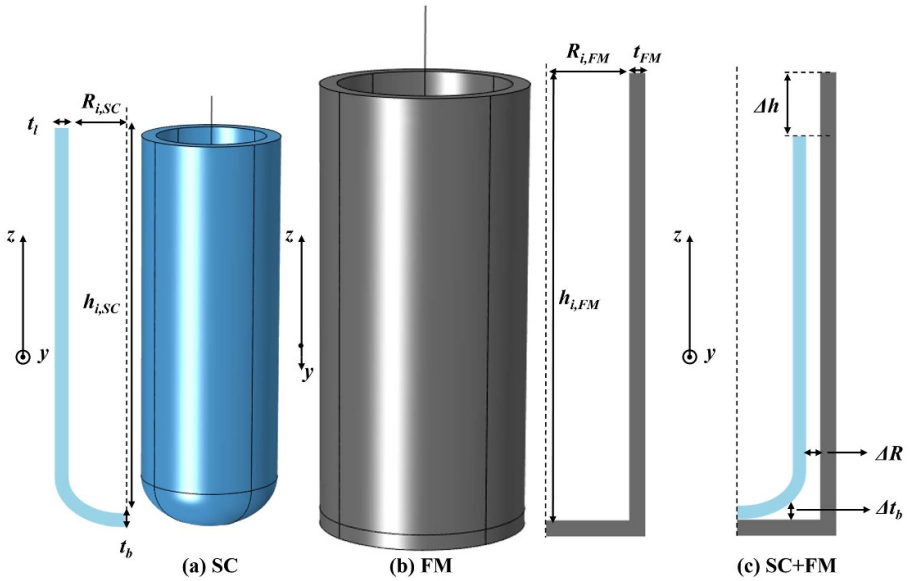


Figure 1. Schematic views of the shielding arrangements: (a) the SC Bi-2223 cup; (b) the FM iron cup; and (c) the coaxial assembly of the SC and FM cups forming the SC+FM shield. The dimensions, radial gap ΔR, axial offset Δh and axial gap Δt_b are reported in the main text.

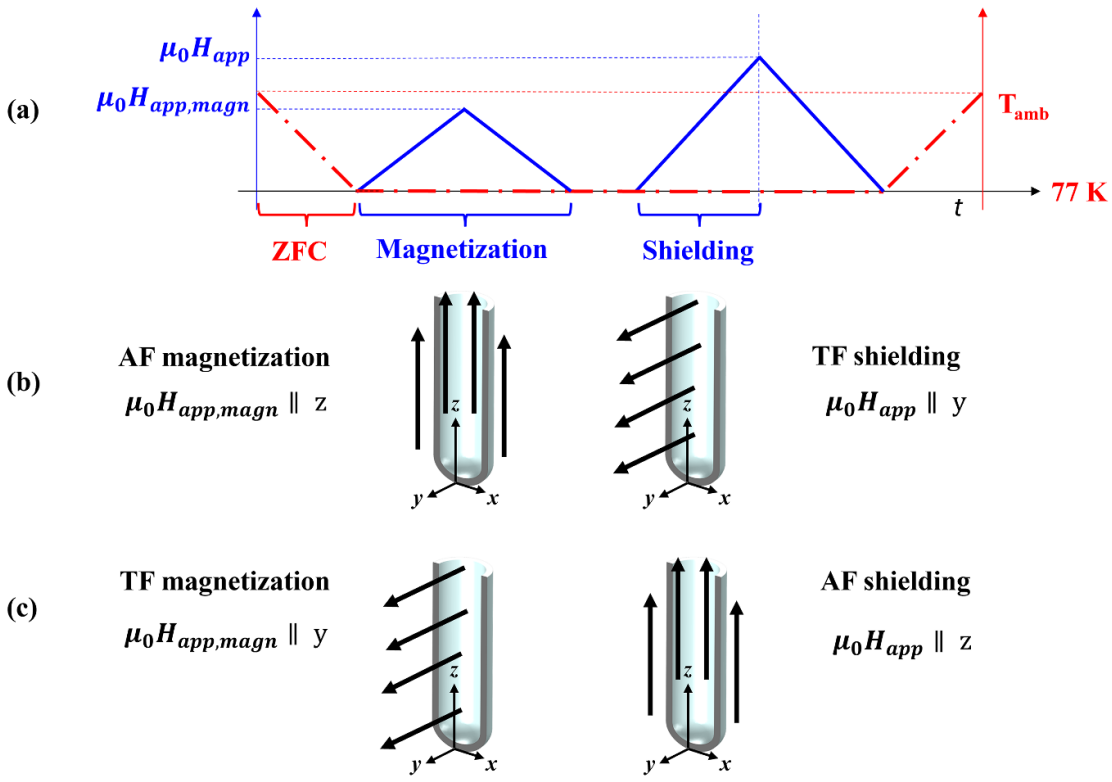


Figure 2. Schematic representation of the cross-field procedures followed in the experiments and numerical calculations: (a) temperature (dashed-dot red line, right axis) and applied-field sequence (blue line, left axis). After zero-field cooling to 77 K, the magnetizing field was increased up to $\mu_0 H_{app,magn}$ and then reduced to zero before the shielding field $\mu_0 H_{app}$ was applied in the perpendicular direction; (b) axial magnetization followed by transverse shielding characterization; (c) transverse magnetization followed by axial shielding characterization.

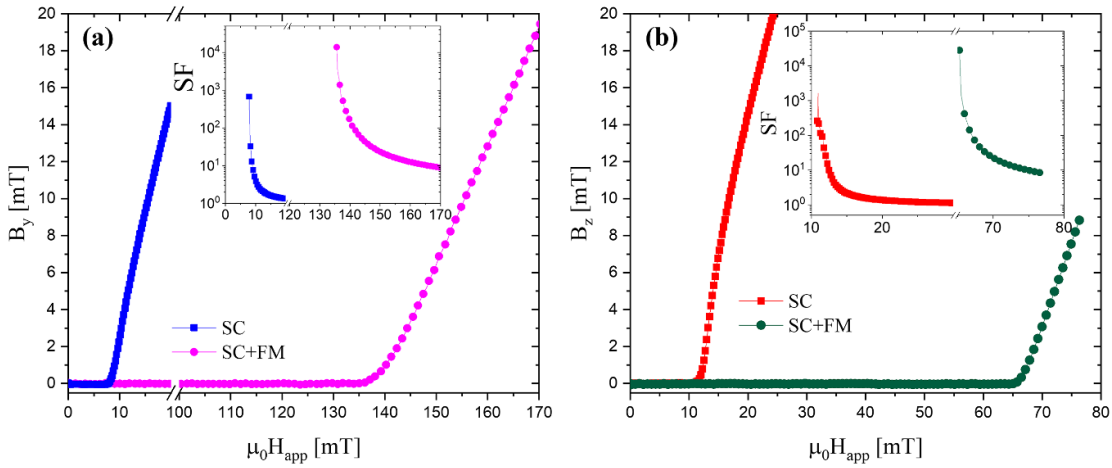


Figure 3. Main panels: magnetic flux density B_y measured in TF orientation (a) and B_z measured in AF orientation (b) at position hp_0 for both SC and SC+FM shields. Insets: corresponding shielding factor (SF) in TF (a) and AF (b) orientations.

3. Experimental results

3.1. AF and TF orientations

The main panels of figures 3(a) and (b) show the magnetic flux density measured after ZFC at position hp_0 on the axis of both the SC (blue and red square symbols) and hybrid shield (magenta and green circular symbols). The measurements were performed as a function of the applied magnetic field, $\mu_0 H_{app}$, at 77 K and for both TF (figure 3(a)) and AF (figure 3(b)) orientations. To quantify the shielding capability of the cup, we introduce the parameter $\mu_0 H_{app,lim}$, defined as the value of the applied magnetic field at which the shielding factor (SF), given by $\mu_0 H_{app}/|B|$ and shown in the insets of figure 3, decreases below a threshold value, arbitrarily set to 50. Accordingly, the SC cup is able to shield the external field up to 8.2 mT and 11.5 mT in the TF and AF orientations, respectively. As expected, the addition of the outer FM cup improves the value of $\mu_0 H_{app,lim}$ in both TF and AF orientations. In particular, $\mu_0 H_{app,lim} = 144$ mT was reached in TF and $\mu_0 H_{app,lim} = 68$ mT in AF orientation.

3.2. Shielding in CF orientation

For the CF characterization, the SC and SC+FM shields were first magnetized (in AF or TF orientations) by applying different magnetic fields $\mu_0 H_{app,magn}$, with values close to the corresponding $\mu_0 H_{app,lim}$ values measured in ZFC condition and hereafter denoted as $\mu_0 H_{app,lim,0}$. The shielding performance of the SC and hybrid cups was then investigated under an applied field perpendicular to the magnetizing one.

For clarity, in the following the subscripts and superscripts of the general quantities $\mu_0 H_{app,magn}$, $\mu_0 H_{app,lim}$, and $\mu_0 H_{app,lim,0}$ indicate the field orientation (AF or TF) and the type of shield (SC or SC+FM), respectively.

3.2.1. AF magnetization and TF shielding

The applied magnetic field values used for AF magnetization of the Bi-2223 cup are shown in figure 4(a), while figure 4(b) reports the corresponding shielding curves obtained after each magnetization cycle. The same procedure was followed for the SC+FM shield, with magnetizing fields shown in figure 5(a) and the resulting shielding curves in figure 5(b).

For both the SC and SC+FM shields, the shielding performance worsens after the magnetization processes. To evaluate their effect on the shielding performance of both the SC and hybrid shields, we introduce two normalized parameters, α_{AF} and β_{TF}, defined as:

$$\alpha_{AF} = \frac{H_{app,magn,AFi}}{H_{app,lim,AF0}} \qquad \beta_{TF} = \frac{H_{app,lim,TFi}}{H_{app,lim,TF0}}. \tag{1}$$

Here, $H_{app,magn,AFi}$ is the applied field used during the ith magnetization process in AF orientation, while $H_{app,lim,AF0}$ is the limit field measured in AF in ZFC condition. Similarly, $H_{app,lim,TFi}$ denotes the limit field measured in TF orientation after the ith magnetization step, and $H_{app,lim,TF0}$ is the reference value obtained in TF without pre-magnetization.

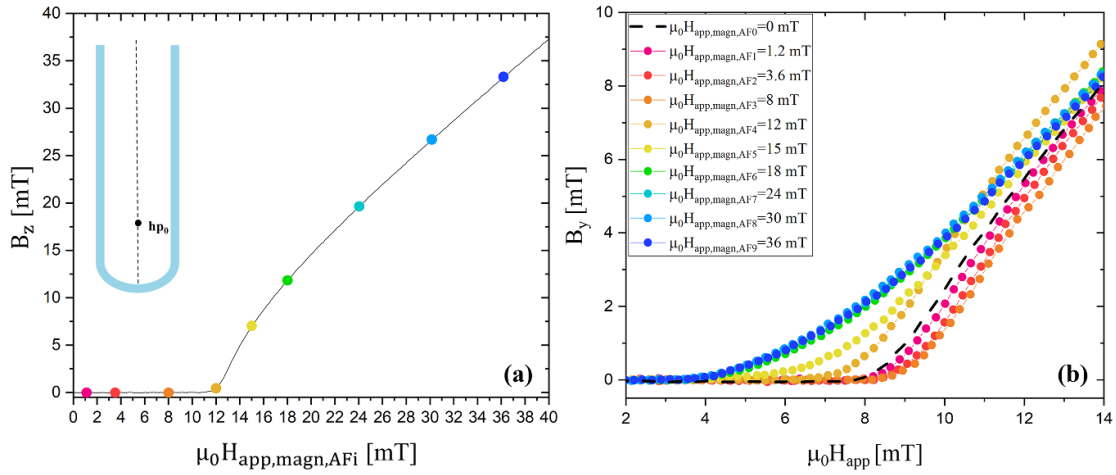


Figure 4. For the SC shield: (a) magnetic flux density, B_z, measured at position hp_0 as a function of the field $\mu_0 H_{\mathrm{app,magn,AF}i}$ applied in the AF magnetization process; (b) magnetic flux density B_y measured at the same position in TF orientation after each magnetization process. Equal colours in panels (a) and (b) identify B_z and B_y values measured during the AF magnetization process (a) and the subsequent TF shielding test.

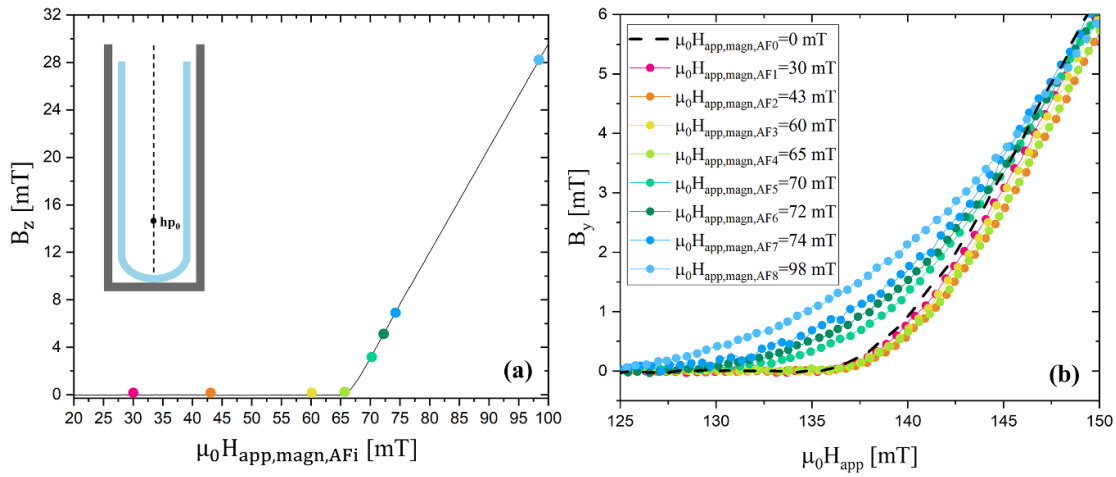


Figure 5. For the SC+FM shield: (a) magnetic flux density, B_z, measured at position hp_0 as a function of the field $\mu_0 H_{\mathrm{app,magn,AF}i}$ applied in the AF magnetization process; (b) magnetic flux density B_y measured at the same position in TF orientation after each magnetization process. Equal colours in panels (a) and (b) identify B_z and B_y values measured during the AF magnetization process (a) and the subsequent TF shielding test.

The parameter α_{AF} (β_{TF}) therefore quantifies the strength of the magnetization process, normalized to the intrinsic shielding capability of the sample in AF (TF) orientation.

Table 1 summarizes the values of $H_{\mathrm{app,magn,AF}i}$ and the corresponding α_{AF} used for the CF characterization for both SC and hybrid shields. By definition, $\alpha_{\mathrm{AF}} = 0$ corresponds to the non-pre-magnetized condition ($H_{\mathrm{app,magn,AF}} = 0$ mT), for which $H^{\mathrm{SC}}_{\mathrm{app,lim,AF0}} = 11.5$ mT and $H^{\mathrm{SC+FM}}_{\mathrm{app,lim,AF0}} = 68$ mT were obtained for the SC and hybrid configurations, respectively.

As already highlighted in figures 4 and 5, the shielding efficiency generally decreases with increasing α_{AF}. Consequently, the $H_{\mathrm{app,lim,TF}i}$ values measured after each magnetization cycle decrease as α_{AF} increases. This behaviour is observed for both SC and hybrid shields. The effect of pre-magnetization on the shielding performance is further illustrated in figure 6, where the dependence of β_{TF} on α_{AF} is reported.

Figure 6 reveals a clear trend. For the SC cup (blue symbols), three distinct regions can be identified:

- $0 < \alpha_{\mathrm{AF}} < 0.70$: $H_{\mathrm{app,lim,TF}}$ slightly improves but remains comparable to the value observed in the non-pre-magnetized configuration;
- $0.70 < \alpha_{\mathrm{AF}} < 1.56$: $H_{\mathrm{app,lim,TF}}$ progressively decreases;

Table 1. $H_{app,magn,AFi}$ values applied in the AF magnetization processes and corresponding α_{AF} values.

(a) SC shield		(b) SC+FM shield	
$H^{SC}_{app,magn,AFi}$ [mT]	α_{AF}	$H^{SC+FM}_{app,magn,AFi}$ [mT]	α_{AF}
0	0	0	0
1.2	0.10	30	0.44
3.6	0.30	43	0.63
8.0	0.70	60	0.88
12	1.04	65	0.96
15	1.36	70	1.03
18	1.56	72	1.06
24	2.09	74	1.09
30	2.61	98	1.44
36	3.13		

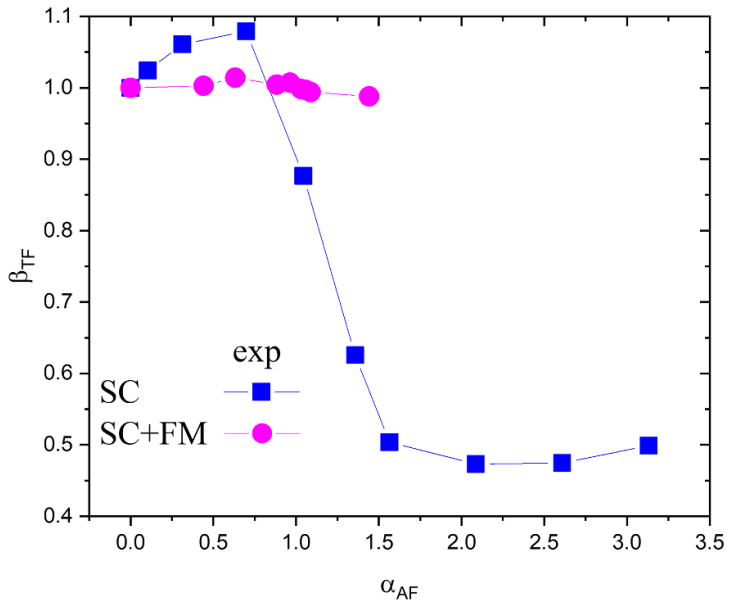


Figure 6. β_{TF} behaviour as a function of α_{AF} for SC (blue square symbols) and SC+FM (magenta circular symbols) shields.

- $\alpha_{AF} > 1.56$: $H_{app,lim,TF}$ shows again a constant trend but its value is half of that measured in ZFC condition.

The addition of the outer FM cup significantly mitigates the effect of the pre-magnetization process. Indeed, the β_{TF} values obtained for the hybrid configuration remain close to 1 (figure 6), indicating that $H_{app,lim,TFi}$ is weakly affected by the pre-magnetization process. However, measurements for $\alpha_{AF} > 1.44$ (i.e. $H_{app,magn,AF} > 98$ mT) could not be performed because of the 98 mT operating limit of the solenoidal electromagnet used in the AF configuration, imposed by coil heating. This regime will be further investigated through numerical simulations.

3.2.2. TF magnetization and AF shielding

The complementary CF configuration is now considered. Figures 7 and 8 show the magnetic flux density, B_y, measured in TF orientation during the pre-magnetization fields (left panels) and the subsequent shielding curves in AF orientation (right panels) for the SC and hybrid shields, respectively.

As in the previous section, we define two analogous α and β parameters for the case of magnetization in TF orientation and shielding characterization in AF orientation:

$$\alpha_{TF} = \frac{H_{app,magn,TFi}}{H_{app,lim,TF0}} \qquad \beta_{AF} = \frac{H_{app,lim,AFi}}{H_{app,lim,AF0}}. \tag{2}$$

Here, $H_{app,magn,TFi}$ is the applied field used during the ith magnetization process in TF orientation, while $H_{app,lim,TF0}$ is the corresponding limit field measured in TF after ZFC. Similarly, $H_{app,lim,AFi}$ denotes

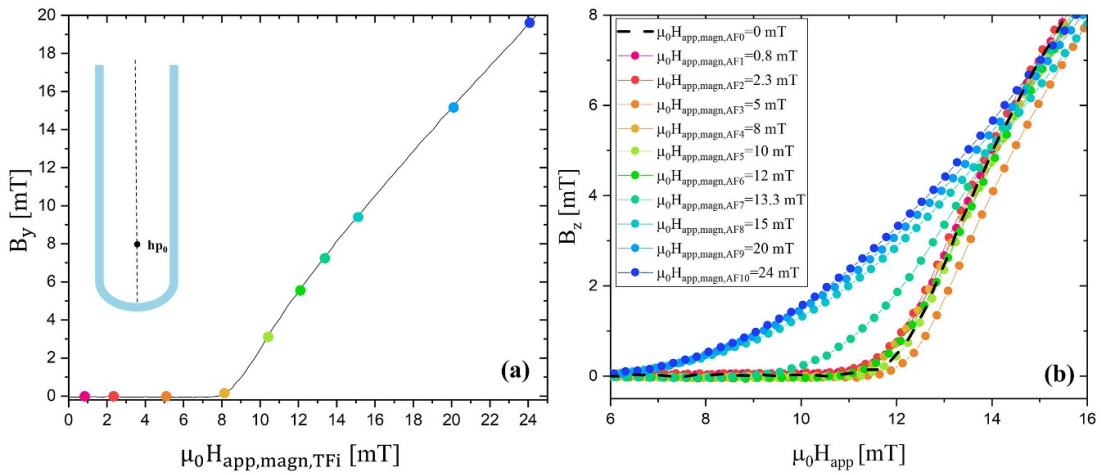


Figure 7. For the SC shield: (a) magnetic flux density, B_y, measured at position hp_0 as a function of the field $\mu_0 H_{\mathrm{app,magn,TF}i}$ applied in the TF magnetization process; (b) magnetic flux density B_z measured at the same position in AF orientation after each magnetization process. Equal colours in panels (a) and (b) identify B_y and B_z values measured during the TF magnetization process (a) and the subsequent AF shielding test.

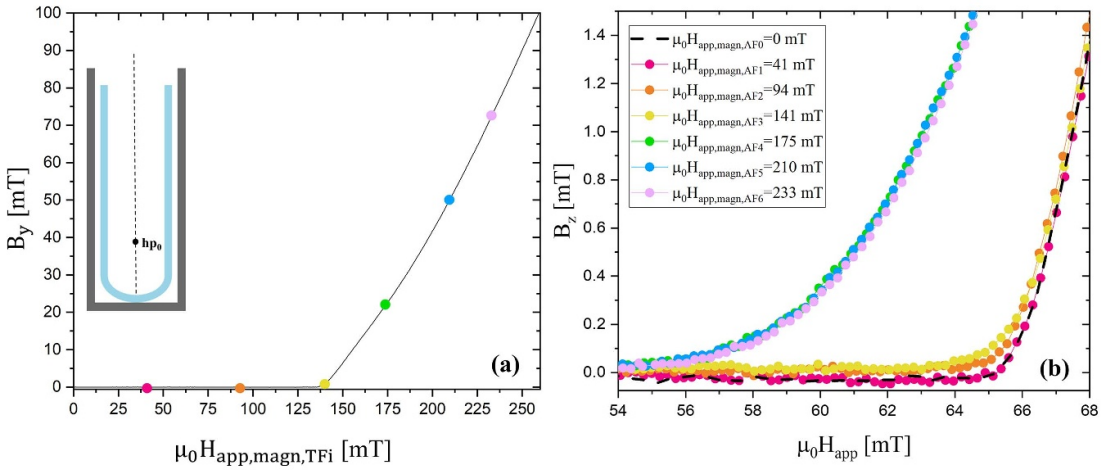


Figure 8. For the SC+FM shield: (a) magnetic flux density, B_y, measured at position hp_0 as a function of the field $\mu_0 H_{\mathrm{app,magn,TF}i}$ applied in the TF magnetization process; (b) magnetic flux density B_z measured at the same position in AF orientation after each magnetization process. Equal colours in panels (a) and (b) identify B_y and B_z values measured during the TF magnetization process (a) and the subsequent AF shielding test.

the limit field measured in AF orientation after the ith magnetization process, and $H_{\mathrm{app,lim,AF0}}$ is the reference value obtained in AF without pre-magnetization.

For the SC shield, $H^{\mathrm{SC}}_{\mathrm{app,lim,TF0}} = 8.2$ mT, whereas $H^{\mathrm{SC+FM}}_{\mathrm{app,lim,TF0}} = 144$ mT was achieved for the hybrid configuration. Table 2 summarizes the values of $H_{\mathrm{app,magn,TF}i}$ and the corresponding α_{TF} used for the CF characterization for both SC and hybrid shields.

As in the previous CF characterization, the shielding performance of the SC cup in AF deteriorates as α_{TF} increases. The dependence of β_{AF} on α_{TF} is reported in figure 9.

Three distinct regions can still be identified for the SC shield:

- $0 < \alpha_{TF} < 1.47$: $H_{\mathrm{app,lim,AF}}$ remains comparable to the non-pre-magnetized case;
- $1.47 < \alpha_{TF} < 1.84$: $H_{\mathrm{app,lim,AF}}$ decreases;
- $\alpha_{TF} > 1.84$: $H_{\mathrm{app,lim,AF}}$ shows a constant trend.

Even in this case, the superimposition of the FM cup greatly attenuates the deterioration of the shielding capability of the pre-magnetized shield. However, in this CF configuration a step-like behaviour of β_{AF} can still be appreciated (figure 9) and will be further investigated numerically in the next section.

Table 2. $H_{app,magn,TFi}$ applied in the TF magnetization processes and corresponding α_{TF} values.

(a) SC shield.	
$H^{SC}_{app,magn,TFi}$ [mT]	α_{TF}
0	0
0.8	0.10
2.3	0.28
5.0	0.62
8.0	0.99
10	1.27
12	1.47
13	1.62
15	1.84
20	2.45
24	2.93

(b) SC+FM shield	
$H^{SC+FM}_{app,magn,TFi}$ [mT]	α_{TF}
0	0
41	0.29
94	0.65
141	0.98
175	1.21
210	1.46
233	1.62

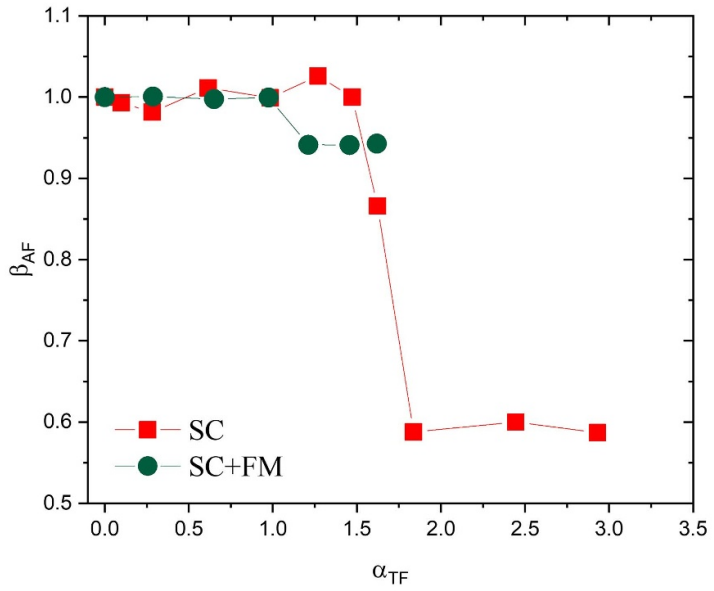


Figure 9. β_{AF} behaviour as a function of α_{TF} for SC (red square symbols) and SC+FM (green circular symbols) shields.

4. Modelling

3D simulations were implemented to reproduce the experimental data collected in ZFC condition in both AF and TF orientations and in both CF experiments. The numerical model was implemented by the finite element software COMSOL 5.6 Multiphysics® [52] through the magnetic field interface (*mf*). The electromagnetic behaviour of the SC, the FM and the surrounding domains were described by solving Maxwell's equations based on the **A**-formulation [50]. Hence, being $\mathbf{B} = \nabla \times \mathbf{A}$ and $\mathbf{E} = -\partial\mathbf{A}/\partial t - \nabla V$, Ampere's equation becomes:

$$\sigma(E)\frac{\partial \mathbf{A}}{\partial t} + \nabla \times \left(\frac{1}{\mu_0 \mu_r}\nabla \times \mathbf{A}\right) = -\sigma(E)\nabla V \tag{3}$$

where μ_r is the relative magnetic permeability (set to 1 in the SC domain) and $\sigma(E) = J(E)/E$ is the electric conductivity depending on the characteristic *E-J*. The SC behaviour was modelled using the power law expression between the current density and the electric field, according to [53]. However, since the equations are formulated as a function of the vector potential **A**, a non-conventional form for the power law equation was used, i.e. the relation $\mathbf{J} = \sigma\mathbf{E}$, proposed in the Ampere Law module in

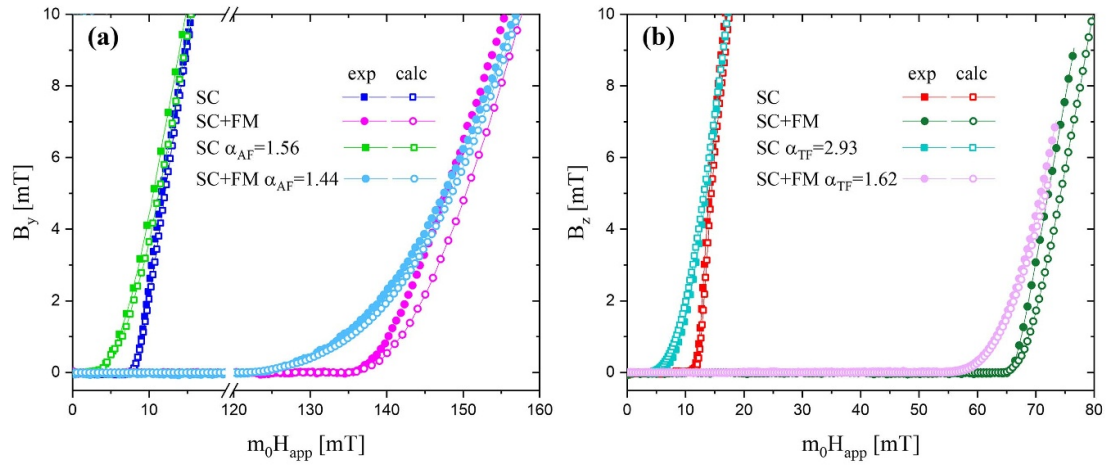


Figure 10. Comparison between the magnetic flux density measured (closed symbols) and calculated (open symbols) for the SC and SC+FM shields in AF (a) and TF (b) orientations, respectively.

Comsol, was customized by directly introducing the *E-J* power law dependence in the electrical conductivity parameter, which took the form:

$$\sigma(E) = \frac{J_c(B)}{E_0} \cdot \left|\frac{|\mathbf{E}|}{E_0}\right|^{\frac{1-n}{n}}. \tag{4}$$

Taking advantage of the tubular geometry of the samples, the value of J_c, needed to determine the $J_c(B)$ dependence, was calculated from the magnetic induction cycles using the approach proposed by Bartolomé *et al* for finite SC rings [54]. This procedure was applied to the magnetic flux density cycles measured at position (hp_1) (i.e. in correspondence to the SC cup open edge) in the AF orientation. This choice was motivated by the fact that, at that position, the effects of the cup closure can be neglected. In agreement with [55], the experimental $J_c(B)$ curve was then fitted using the Kim equation:

$$J_c(B) = \frac{J_{c0}}{\left(1 + \frac{B}{B_1}\right)} \tag{5}$$

obtaining the fit parameter values $J_{c0} = 1.3 \cdot 10^7$ A m^{-2} and $B_1 = 6.15$ mT.

The n parameter was estimated from a previous *relaxation creep experiment* performed following the procedure described in [53]. This experiment allowed us to obtain the normalized flux creep rate S, related to n by the equation:

$$S = \frac{1}{1-n} \tag{6}$$

S was estimated to be -0.013. Hence, from equation (6), we obtained $n = 76$.

The FM shield was described by introducing the characteristic B–H curve [48]. For both AF and TF orientations, the applied magnetic field $\mathbf{H}_{app}$ was imposed as a boundary condition. Far from the shield, the magnetic flux density was assumed to be $\mathbf{B} = \mu_0\mathbf{H}_{app}$, increasing linearly with a ramp rate of 0.5 mT s^{-1}.

To reproduce the CF experiments, the magnetization process was modelled by applying a triangular $\mathbf{B}(\mu_0\mathbf{H}_{app})$ waveform with amplitude $A = \mu_0 H_{app,magn}$. The resulting magnetization state of the sample was then used as the initial condition for the subsequent simulations of the AF or TF shielding experiment.

4.1. Modelling validation

The first validation of the model was carried out by comparing the computational results with the experimental data for both the field orientations, AF and TF, and in both ZFC and CF pre-magnetization conditions. To this aim, the magnetic flux density was determined at the same position hp_0 as in the experimental setup following the same magnetic history. The comparisons between the computational and experimental results achieved after the ZFC and CF pre-magnetization for the

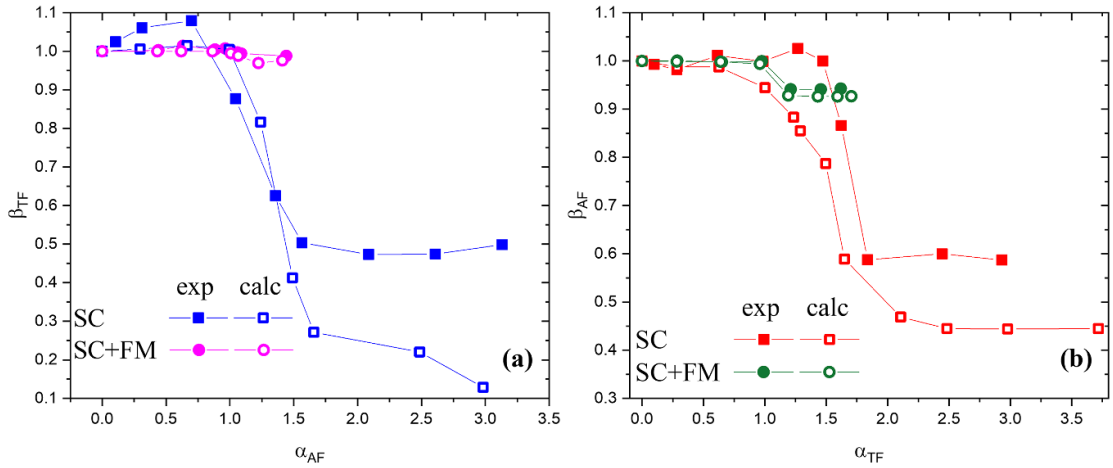


Figure 11. Comparison between the experimental (closed symbols) and calculated (open symbols) β_{TF} vs α_{AF} (a) and β_{AF} vs α_{TF} (b) curves for the SC (blue and red squares) and SC+FM (magenta and green circles) shields.

SC and hybrid shields are shown in figure 10 for (a) AF orientation and (b) TF orientation. In both field orientations, the results closely match the experimental measurements. For the sake of clarity, only one value of α for each shield and CF characterization is shown in figure 10, i.e. $\alpha_{AF} = 1.56$ and $\alpha_{TF} = 2.93$ for the SC shield and $\alpha_{AF} = 1.44$ and $\alpha_{TF} = 1.62$ for the SC+FM shield.

Figures 11(a) and (b) compare the β vs α curves measured and calculated for the SC and SC+FM shields after AF and TF magnetization, respectively. α and β are defined as in section 3.2.

Despite a slight underestimation of the experimental values, the model qualitatively reproduces the effect of the magnetization process on the shielding performance. This could be ascribed to the fact that both configurations involved the application of a transverse magnetic field (during the magnetization process or during the shielding properties investigation). In this field orientation, the presence of geometrical inhomogeneities and surface roughness (not considered in the model) is expected to have a greater influence on the magnetic response of the shield than in axial orientation [56]. Nevertheless, given the overall agreement between numerical and experimental data, we can conclude that the model provides a useful tool to further investigate the influence of the magnetization history on the shielding properties.

4.2. Modelling results

Based on this validation, the model was further employed to investigate magnetization conditions that could not be explored experimentally and to gain insight into the mechanisms responsible for the degradation of the shielding performance after CF magnetization.

First, the effect of the AF magnetization on the shielding performance of the hybrid shield was evaluated for $\mu_0 H_{app,magn,AF} > 98$ mT. In particular, $\mu_0 H_{app,magn,AF}$ values of 110 mT and 200 mT were considered, corresponding to $\alpha_{AF} = 1.58$ and $\alpha_{AF} = 2.88$, respectively. The results shown in figure 12(a) confirm that β_{TF} reaches a plateau for $\alpha_{AF} > 1.44$.

Then, we investigated the step-like behaviour of β_{AF} in the SC+FM shield magnetized in TF orientation. β_{AF} was calculated for $\mu_0 H_{app,magn,TF} = 155$ mT ($\alpha_{TF} = 1.05$). Confirming the output of the experimental characterization, the additional β_{AF} value lies on the descending branch of the curve (figure 12(b)).

To elucidate the influence of the magnetization process on the shielding performance, the distributions of the magnetic field and, consequently, of the current density flowing in the material were analysed under ZFC and CF pre-magnetization conditions. We focused on TF shielding capability after AF magnetization. The first row of figure 13 reports the 2D magnetic flux density distribution on the *xz*-plane cross-section after AF magnetization up to $\mu_0 H_{app,magn,AF} = 8$ mT and $\mu_0 H_{app,magn,AF} = 18$ mT. These applied field values correspond to $\alpha_{AF} = 0.70$ and $\alpha_{AF} = 1.56$, respectively, i.e. to conditions below and above the transition region between the two plateaus observed in the β_{TF} vs α_{AF} curve (figure 11(a)). The second row illustrates the corresponding 3D current density distribution within the superconductor, displayed on the half-volume with $x < 0$, together with the current flow direction shown for $x > 0$. Notice that the schematics reported in the first column of figure 13 are displayed in perspective view to highlight the coordinate system and observation geometry, whereas the maps shown in the

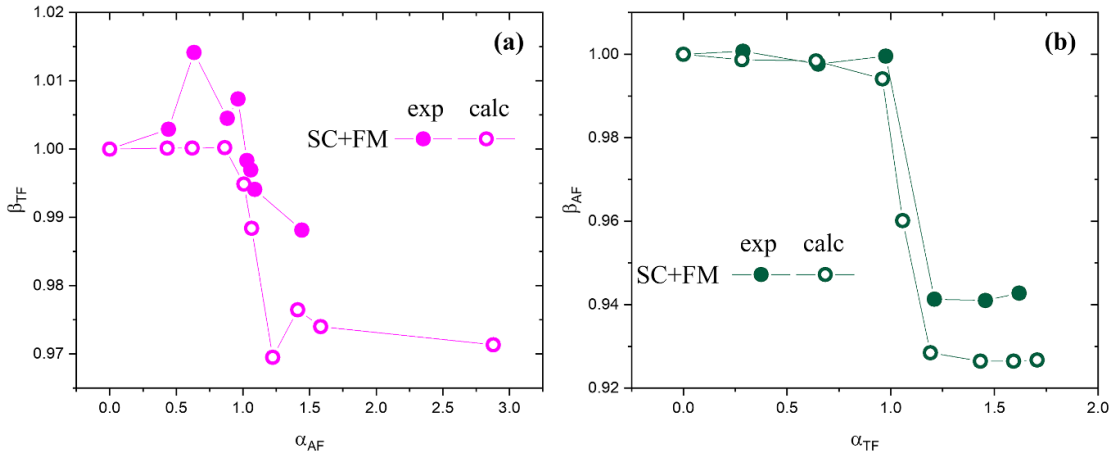


Figure 12. Calculated β_{TF} vs α_{AF} (a) and β_{AF} vs α_{TF} (b) curves for hybrid shield with the additional point calculated assuming $\alpha_{AF} = 1.58$ and $\alpha_{AF} = 2.88$ (a), and $\alpha_{TF} = 1.05$ (b).

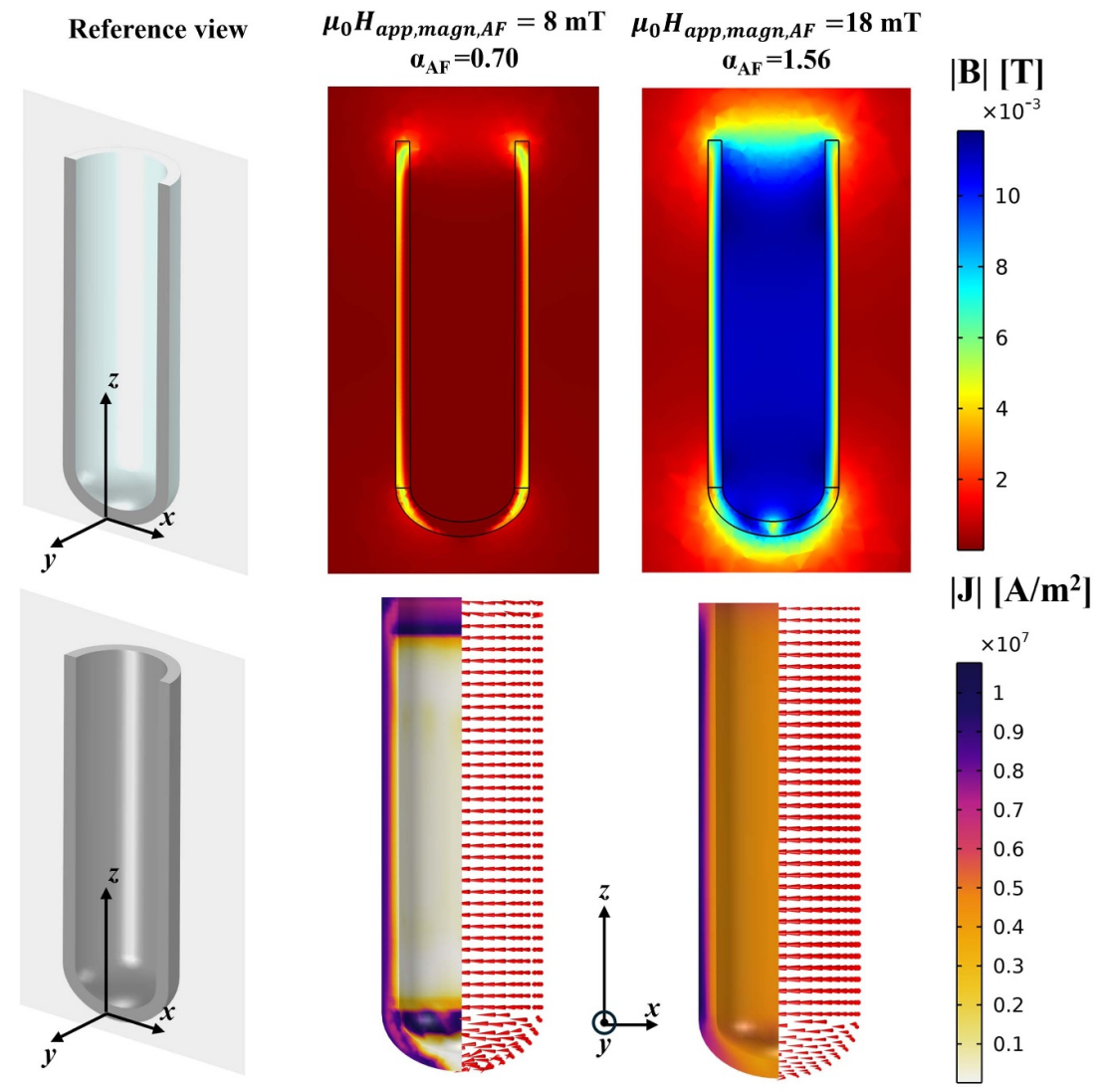


Figure 13. 2D magnetic flux density (upper row) and 3D current density distribution (bottom row) for the SC shield after an AF magnetization process up to $\mu_0 H_{app,magn,AF} = 8$ mT ($\alpha_{AF} = 0.70$) and 18 mT ($\alpha_{AF} = 1.56$) and subsequent field removal. The AF was applied along the *z*-direction. The first column reports the viewing geometry in perspective view, while the maps displayed in the second and third columns are shown frontally with respect to the *xz*-plane.

second and third columns are viewed frontally with respect to the *xz*-plane. As expected, the remanent field obtained for $\alpha_{AF} = 1.56$ is higher than that for $\alpha_{AF} = 0.70$; in particular, the maximum magnetic flux densities observed inside the material are approximately 9 mT and 5 mT respectively. The higher pre-magnetization field results in a deeper penetration of the magnetic field into the superconductor and, hence, in a greater current density distribution. In particular, for $\alpha_{AF} = 0.70$, the current density reaches values close to 1×10^7 A m^{-2} near the edge of the cup, indicating stronger currents in regions where flux penetration is more pronounced. Conversely, for $\alpha_{AF} = 1.56$, the current density is more homogeneous throughout the sample, reaching values close to 0.5×10^7 A m^{-2} on the inner surface and up to 1×10^7 A m^{-2} on the outer surface. However, in both cases, the current predominantly flows tangentially to the lateral surface of the cup, as expected for this applied field orientation. This difference in current density magnitude after the magnetization process leads to a different response of the shield under a subsequent TF-oriented field application. In particular, higher magnetization reduces the ability of the superconductor to sustain additional shielding currents when a TF is applied, thereby contributing to the observed degradation of the shielding performance.

The impact of these initial conditions on the TF shielding is further illustrated in figure 14. Here, the upper row shows the magnetic flux density distribution under a TF $\mu_0 H_{app} = 6$ mT applied along the *y*-direction of the zero field cooled ($\alpha_{AF} = 0$) and of the pre-magnetized shield at $\mu_0 H_{app,magn,AF} = 8$ mT ($\alpha_{AF} = 0.70$) and $\mu_0 H_{app,magn,AF} = 18$ mT ($\alpha_{AF} = 1.56$). The viewing geometries are the same as those shown in figure 13. A clear evolution of the shielding performance can be observed. In the absence of pre-magnetization, the applied TF is largely shielded by the superconductor. In contrast, the AF magnetization at increasing fields leads to a progressive flux line penetration inside the cup preferentially from the open end. This effect is more pronounced for $\alpha_{AF} = 1.56$, where a higher magnetic flux density distribution is observed. This affects the current distribution in the shield wall in a way consistent with what is already shown in figure 13: the presence of trapped magnetic flux limits the additional shielding currents that can be supported in TF orientation, thus leading to a less effective magnetic shielding. As a result, the magnetic flux density in the inner region of the shield increases with the value of magnetization field, providing a consistent physical interpretation of the reduction in shielding performance and the different magnetization behaviour observed between the two plateaus in the β_{TF} curve.

A further difference emerges in the orientation of the current density, reflecting the competition between the current patterns induced by the AF magnetization and those generated by the subsequent TF. In the ZFC case, as expected for TF shielding, the shielding currents flow predominantly parallel to the shield's axis. In contrast, in the AF pre-magnetized configurations, the current distribution retains a memory of the previously established current loops. The magnetization-induced currents, arranged in closed circular paths, interact with the shielding currents generated by the application of TF, leading to a distortion of the overall current pattern and to regions where the current direction deviates from the axial one. For $\alpha_{AF} = 0.70$, the perturbation remains limited, and the current density progressively reorients towards the configuration imposed by the TF. Conversely, when $\alpha_{AF} = 1.56$, the current distribution is significantly altered, with current loops following trajectories that deviate from those typically associated with purely axial or transverse applied fields. This interplay between magnetization-induced and shielding currents explains the degradation of the shielding performance, evidencing how part of the available current-carrying capacity is already engaged in sustaining the pre-existing flux distribution.

It is well known that the addition of the FM shield prevents the penetration of the applied field into the superconductor [46, 48]. In the absence of previous magnetization, this results in a clear improvement of the shielding performance. In contrast, when a TF field is applied to the sample already pre-magnetized in AF, the FM shield hinders the reorientation of the current density within the superconductor. Figure 15 shows the current density magnitude distribution and flow direction in the SC+FM shield under conditions comparable to those of figure 14. In particular, an applied TF $\mu_0 H_{app} = 110$ mT is considered in three cases: a non-magnetized superconductor, a superconductor pre-magnetized in AF up to $\mu_0 H_{app,magn,AF} = 43$ mT and $\mu_0 H_{app,magn,AF} = 110$ mT. These magnetization levels correspond to $\alpha_{AF} = 0.63$ and $\alpha_{AF} = 1.58$, respectively, the latter value being calculated from the computational output. Additionally, these values were chosen consistently with those considered for the SC-only configuration, i.e. $\mu_0 H_{app,magn,AF}$ values ensuring full magnetic shielding and α_{AF} values representative of the two plateaus discussed above (see figure 11(a)). For $\alpha_{AF} = 0.63$, the current density distribution is similar to that of the non-magnetized sample, with higher values near the open edge of the SC cup due to field penetration from the opening of the FM shield. Conversely, for $\alpha_{AF} = 1.58$, the current density becomes more homogeneous throughout the SC, while its direction remains that imposed by an AF. This suggests that the FM shield slows down the reorientation process of the current density under TF, so that it occurs only when the applied field is already close to the intrinsic shielding limit of the hybrid system.

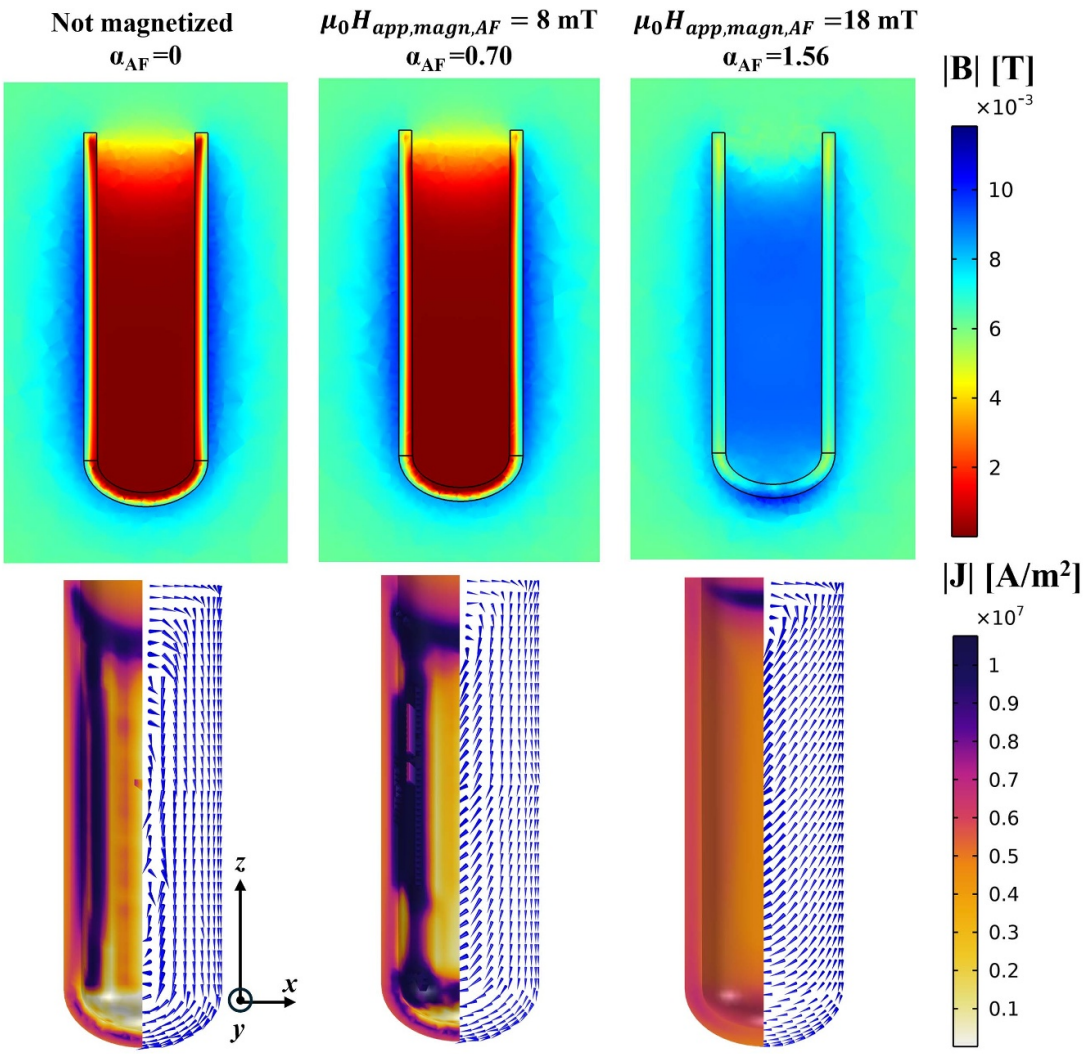


Figure 14. Magnetic flux density (upper row) and current density magnitude and orientation (bottom row) in SC shield after the AF magnetization cycle up to $\mu_0 H_{\mathrm{app,magn,AF}} = 8$ mT ($\alpha_{\mathrm{AF}} = 0.70$) and 18 mT ($\alpha_{\mathrm{AF}} = 1.56$) followed by the application of a transverse field, $\mu_0 H_{\mathrm{app}} = 6$ mT, along the y-direction.

Although not explicitly shown here, the same physical mechanisms are expected to govern the complementary CF characterization, i.e. TF magnetization followed by AF shielding, resulting in a similar interplay between magnetization-induced and shielding currents and, consequently, in an analogous impact on the shielding performance.

5. Conclusion

In this work, the DC magnetic shielding properties of a commercial Pb-doped Bi-2223 single-capped tube with a hemispherical end were investigated experimentally and numerically under axial, transverse, and CF configurations. The effect of a FM layer was further assessed by considering a hybrid SC+FM layout. The results demonstrate that the shielding response of the SC cup is strongly dependent on its magnetic history. In particular, the pre-magnetization progressively degrades the shielding capability under magnetic fields applied perpendicular to the magnetizing direction, revealing three distinct regimes associated with the evolution of the current distribution within the superconductor. Indeed, after an initial steady trend indicating the negligible effect of the pre-magnetizing process, the β parameter used to quantify the influence of the CF magnetization exhibit a progressive decrease followed by a second plateau as the pre-magnetization field is increased. This behaviour qualitatively agrees with that previously reported by Wéra *et al* [41] for an open Bi-2223 tube. The present results therefore confirm that the magnetic history effects identified in the open tubular geometry also occur in a single-capped

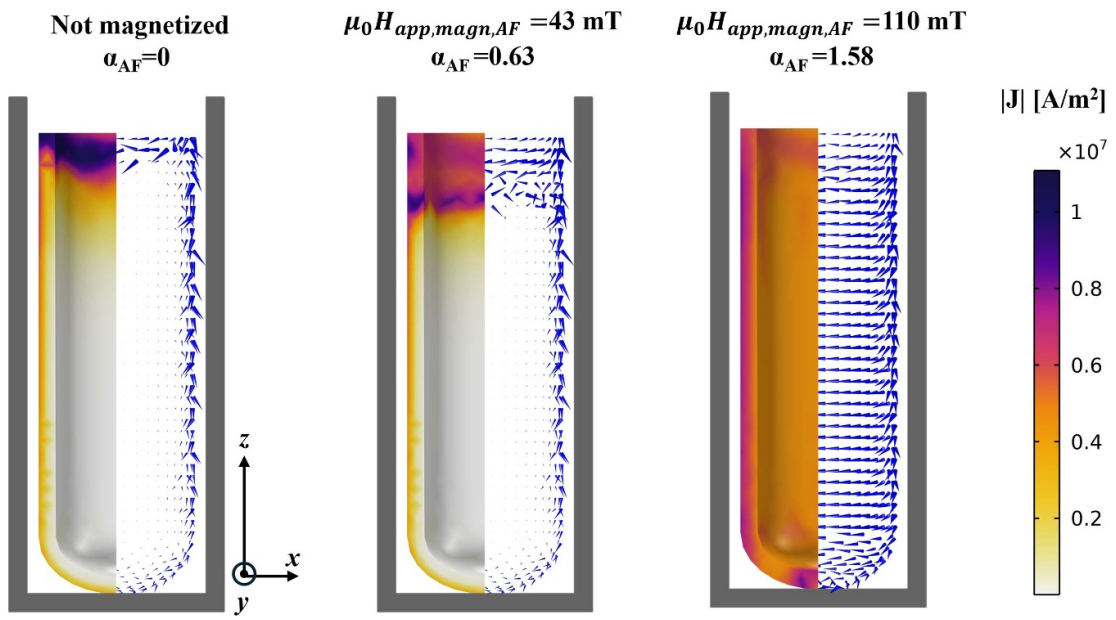


Figure 15. 3D current density distribution and current flow direction in SC+FM shield calculated assuming a transverse field $\mu_0 H_{app} = 110$ mT applied along the y-direction under ZFC condition (left), after an AF pre-magnetization cycle up to $\mu_0 H_{app,magn,AF} = 43$ mT ($\alpha_{AF} = 0.63$) and up to 110 mT ($\alpha_{AF} = 1.58$).

tube, despite the different geometry and the three-dimensional end effects introduced by its hemispherical closed bottom. In contrast, the superimposition of the FM cup significantly reduces these history-dependent effects, preserving an almost unchanged shielding capability over a considerably wider range of pre-magnetizing fields. The outer FM cup thus improves not only the shielding performance under zero-field-cooled conditions but also its stability against changes in the magnetic history. The numerical model, based on the **A**-formulation, was validated through the comparison with the experimental data and successfully reproduced both the shielding behaviour and its degradation after CF magnetization processes. The simulations provide physical insight into the underlying mechanisms, showing that the interaction between magnetization-induced currents and shielding currents leads to a redistribution of the current density loops, thereby limiting the additional shielding capability of the superconductor. Overall, these findings evidence the role of magnetization history in HTS magnetic shielding and demonstrate the effectiveness of hybrid SC+FM configurations in mitigating its detrimental effects. The combined experimental and numerical approach developed in this work may provide a useful basis for the design and optimization of SC shielding systems operating in complex magnetic environments.

Acknowledgments

This study was carried out within the Space It Up project funded by the Italian Space Agency, ASI, and the Ministry of University and Research, MUR, under Contract No. 2024–5-E.0 - CUP No. I53D24000060005.

Data availability statement

All data that support the findings of this study are included within the article (and any supplementary files).

ORCID iDs

M Fracasso 0000-0002-6339-4188
R Gerbaldo 0000-0002-6543-864X
G Ghigo 0000-0003-3368-1319

J-F Fagnard 0000-0002-8898-0298
P Vanderbemden 0000-0002-1436-7116
L Gozzelino 0000-0002-9204-0792

References

[1] Yu K K, Lee Y H, Lee S J, Shim J H, Hwang S, Kim J M, Kwon H and Kim K 2014 *Supercond. Sci. Technol.* **27** 105007
[2] Brandl M *et al* 2016 *Rev. Sci. Instrum.* **87** 113103
[3] Hinterberger A, Gerber S and Doser M 2017 *J. Instrum.* **12** T09002
[4] Wei L, Wang G, Li J, Zhang S and Hong G 2021 *J. Instrum.* **16** P04007
[5] He S and Zheng J 2024 *IEEE Trans. Appl. Supercond.* **34** 3602504
[6] Visser L, Neis M, Guimaraes J R, Jerger M, Bushev P, Barends R and Mourik V 2024 *Two-Stage Magnetic Shielding for Hybrid Quantum Devices in an Adiabatic Demagnetization Refrigerator* (*Silicon Quantum Electronics Workshop 2024, Davos (Switzerland), 4–6 September 2024*) (https://doi.org/10.34734/FZJ-2025-00490)
[7] Pourrahimi S, Williams J, Punchard W, Tuttle J, DiPirro M, Canavan E and Shirron P 2008 *Cryogenics* **48** 253–7
[8] Wu B, Wang Z, Cheng B, Wang Q, Xu A and Lin Q 2014 *Metrologia* **51** 452
[9] Körber R, Storm J H, Seton H, Mäkelä J P, Paetau R, Parkkonen L, Pfeiffer C, Riaz B, Schneiderman J F and Dong H *et al* 2016 *Supercond. Sci. Technol.* **29** 113001
[10] Wang S, Wang S, Yu X, Xu H, Li Y, Jiang H and Sun K 2023 *Supercond. Sci. Technol.* **36** 035001
[11] Rotheudt N, Fracasso M, Vanderbemden P and Gozzelino L 2025 *Supercond. Sci. Technol.* **38** 043002
[12] Rabbers J J, Oomen M P, Bassani E, Ripamonti G and Giunchi G 2010 *Supercond. Sci. Technol.* **23** 125003
[13] Dbeyssi A, Froelich B, Espi M C M, Maas F, Capozza L, Noll O, Wang Y and Lin D 2023 *Nucl. Instrum. Methods Phys. Res. A* **1050** 168087
[14] Itoh M, Ohyama T, Minemoto T, Numata K and Hoshino K 1992 *J. Phys. D: Appl. Phys.* **25** 1630
[15] Giunchi G, Barna D, Bajas H, Brunner K, Német A and Petrone C 2018 *IEEE Trans. Appl. Supercond.* **28** 6801705
[16] Barna D, Giunchi G, Novák M, Brunner K, Német A, Petrone C, Atanasov M, Bajas H and Feuvrier J 2019 *IEEE Trans. Appl. Supercond.* **29** 4101310
[17] Frankel D 1979 *IEEE Trans. Magn.* **15** 1349–53
[18] Gubser D, Wolf S, Francavilla T, Claassen J and Das B 1985 *IEEE Trans. Magn.* **21** 320–3
[19] Zheng B, Xie W, Liu Y, Zhu X, Ming X, Zhang Y and Wen H H 2024 *IEEE Trans. Appl. Supercond.* **34** 8200910
[20] Hatwar R, Kvitkovic J, Herman C and Pamidi S 2015 *IOP Conf. Ser. Mater. Sci. Eng.* **102** 012012
[21] Kvitkovic J, Patel S, Zhang M, Zhang Z, Peetz J, Marney A and Pamidi S 2018 *IEEE Trans. Appl. Supercond.* **28** 9001705
[22] Strickland N M, Olatunji J R, Shellard C, Huang X, Wimbush S C, Acheson C R, Weijers H and Pollock R 2025 *IEEE Trans. Appl. Supercond.* **35** 1–7
[23] Nagasaki Y, Solovyov M and Göm'ory F 2018 *IEEE Trans. Appl. Supercond.* **28** 6601905
[24] Gupta R *et al* 2019 *IEEE Trans. Appl. Supercond.* **29** 4002104
[25] Plechacek V, Hejtmanek J, Sedmidubsky D, Knizek K, Pollert E, Janu Z and Tichy R 1995 *IEEE Trans. Appl. Supercond.* **5** 528–31
[26] Çelebi S, Gencer A and Öztürk A 1997 *J. Alloys Compd.* **257** 14–18
[27] He A, Hua P, Zhang J, Fu X and Zhou Y 1997 *Physica C* **282-287** 2635–6
[28] Tomków Ł, Ciszek M and Chorowski M 2015 *J. Appl. Phys.* **117** 043901
[29] Dou Y, Gao Y, Wang K, Zhang M, Li J, Fang X, Sun B and Ma D 2026 *Measurement* **259** 119636
[30] Wéra L, Fagnard J F, Hogan K, Vanderheyden B, Namburi D K, Shi Y, Cardwell D A and Vanderbemden P 2019 *IEEE Trans. Appl. Supercond.* **29** 6801109
[31] Mori K, Minemoto T and Itoh M 1997 *IEEE Trans. Appl. Supercond.* **7** 378–81
[32] Yasui K, Tarui Y and Itoh M 2006 Improvement of the magnetic shielding effects by the superposition of a multi-layered ferromagnetic cylinder over an HTS cylinder: relationship between the shielding effects and the layer number of the ferromagnetic cylinder *J. Phys. Conf. Ser.* **43** 1393
[33] Itoh M, Ohyama T, Mori K and Minemoto T 1994 *Cryogenics* **34** 817–20
[34] Itoh M, Pavese F, Mori K, Vanolo M and Minemoto T 1996 *J. Magn. Soc. Japan* **20** 289–92
[35] Tinkham M 2004 *Introduction to Superconductivity* (*Dover Books on Physics Series*) (Dover Publications)
[36] Bean C P 1962 *Phys. Rev. Lett.* **8** 250–3
[37] Brandt E H 1998 *Phys. Rev. B* **58** 6506–22
[38] Vanderbemden P, Hong Z, Coombs T A, Denis S, Ausloos M, Schwartz J, Rutel I B, Hari Babu N, Cardwell D A and Campbell A M 2007 *Phys. Rev. B* **75** 174515
[39] Dadhich A and Pardo E 2020 *Sci. Rep.* **10** 19265
[40] Rotheudt N, Fagnard J F, Hlasek T, Plechacek J and Vanderbemden P 2026 *IEEE Trans. Appl. Supercond.* **36** 1–6
[41] Wéra L, Fagnard J F, Hogan K, Vanderheyden B and Vanderbemden P 2018 *The Influence of an Initial Trapped Field on the Magnetic Shielding Performance of Bulk High-Temperature Superconducting Tubes* (*High-Temperature Superconductors: Occurrence, Synthesis and Applications*) (Nova Science)
[42] Öztürk A and Kara A 2020 *J. Supercond. Nov. Magn.* **33** 3411–6
[43] Sirois F and Grilli F 2015 *Supercond. Sci. Technol.* **28** 043002
[44] Bortot L, Auchmann B, Garcia I C, De Gersem H, Maciejewski M, Mentink M, Schöps S, Van Nugteren J and Verweij A P 2020 *IEEE Trans. Appl. Supercond.* **30** 4900911
[45] Arsenault A, Sirois F and Grilli F 2021 *IEEE Trans. Appl. Supercond.* **31** 6800111
[46] Fracasso M, Gömöry F, Solovyov M, Gerbaldo R, Ghigo G, Laviano F, Napolitano A, Torsello D and Gozzelino L 2022 *Materials* **15** 667
[47] Sirois F, Grilli F and Morandi A 2019 *IEEE Trans. Appl. Supercond.* **29** 8000110
[48] Gozzelino L *et al* 2022 *Supercond. Sci. Technol.* **35** 044002
[49] Stavrev S, Grilli F, Dutoit B, Nibbio N, Vinot E, Klutsch I, Meunier G, Tixador P, Yang Y and Martinez E 2002 *IEEE Trans. Magn.* **38** 849–52
[50] Solovyov M and Gömöry F 2019 *Supercond. Sci. Technol.* **32** 115001

[51] CAN Superconductors (available at: www.can-superconductors.com/hts-bulks-and-materials/bi-2223-magnetic-shields/) (Accessed 28 August 2026)
[52] COMSOL Multiphysics® (available at: www.comsol.com/) (Accessed 22 May 2026)
[53] Fagnard J F, Elschner S, Bock J, Dirickx M, Vanderheyden B and Vanderbemden P 2010 *Supercond. Sci. Technol.* **23** 095012
[54] Bartolomé E, Granados X, Palau A, Puig T, Obradors X, Navau C, Pardo E, Sánchez A and Claus H 2005 *Phys. Rev. B* **72** 024523
[55] Fagnard J F, Dirickx M, Ausloos M, Lousberg G, Vanderheyden B and Vanderbemden P 2009 *Supercond. Sci. Technol.* **22** 105002
[56] Gozzelino L *et al* 2020 *Supercond. Sci. Technol.* **33** 044018